Author(s): Yuwen Pang, Aleksi Räsänen, Viivi Lindholm, Mika Aurela & Tarmo Virtanen

Title: Detecting peatland vegetation patterns with multi-temporal field spectroscopy

Year: 2022

Version: Published version

Please cite the original version:

Yuwen Pang, Aleksi Räsänen, Viivi Lindholm, Mika Aurela & Tarmo Virtanen (2022) Detecting peatland vegetation patterns with multi-temporal field spectroscopy, GIScience & Remote Sensing, 59:1, 2111-2126, DOI: 10.1080/15481603.2022.2152303

GIScience & Remote Sensing

ISSN: (Print) (Online) Journal homepage: https://www.tandfonline.com/loi/tgrs20

Detecting peatland vegetation patterns with multi-temporal field spectroscopy

Yuwen Pang, Aleksi Räsänen, Viivi Lindholm, Mika Aurela & Tarmo Virtanen

To cite this article: Yuwen Pang, Aleksi Räsänen, Viivi Lindholm, Mika Aurela & Tarmo Virtanen (2022) Detecting peatland vegetation patterns with multi-temporal field spectroscopy, GIScience & Remote Sensing, 59:1, 2111-2126, DOI: 10.1080/15481603.2022.2152303

To link to this article: https://doi.org/10.1080/15481603.2022.2152303

GISCIENCE & REMOTE SENSING
2022, VOL. 59, NO. 1, 2111–2126
https://doi.org/10.1080/15481603.2022.2152303

Taylor & Francis
Taylor & Francis Group

Detecting peatland vegetation patterns with multi-temporal field spectroscopy

Yuwen Pang[a], Aleksi Räsänen[b], Viivi Lindholm[a], Mika Aurela[c] and Tarmo Virtanen[a]

[a]Ecosystem and Environment Research Program, Faculty of Biological and Environmental Sciences, University of Helsinki, Helsinki, Finland; [b]Natural Resources Institute Finland (Luke), Finland; [c]Finnish Meteorological Institute, Helsinki, Finland

ABSTRACT

Peatlands are one of the most significant terrestrial carbon pools, and the processes behind the carbon cycle in peatlands are strongly associated with different vegetation patterns. Handheld spectroradiometer data has been widely applied in ecological research, but there is a lack of studies on peatlands assessing how the temporal and spectral resolution affect the detectability of vegetation patterns. We collected field spectroscopy and vegetation inventory data at two northern boreal peatlands, Lompolojänkkä and Halssiaapa, between late May and August 2019. We conducted multivariate random forest regressions to examine the appropriate periods, benefits of multi-temporal data, and optimal spectral bandwidth and sampling interval for detecting plant communities and the two-dimensional (2D) %-cover, above-ground biomass (AGB) and leaf area index (LAI) of seven plant functional types (PFTs). In the best cross-site regression models for detecting plant community clusters (PCCs), R^2 was 42.6–48.0% (root mean square error (RMSE) 0.153–0.193), and for PFT 2D %-cover 53.9–69.8% (RMSE 8.2–17.6%), AGB 43.1–61.5% (RMSE 86.2–165.5 g/m^2) and LAI 46.3–51.3% (RMSE 0.220–0.464 m^2/m^2). The multi-temporal data of the whole season increased R^2 by 13.7–24.6%-points and 10.2–33.0%-points for the PCC and PFT regressions, respectively. There was no single optimal temporal window for vegetation pattern detection for the two sites; in Lompolojänkkä the early growing season between late May and mid-June had the highest regression performance, while in Halssiaapa, the optimal period was during the peak season, from July to early August. In general, the spectral sampling interval between 1 to 10 nm yielded the best regression performance for most of the vegetation characteristics in Lompolojänkkä, whereas the optimal range extended to 20 nm in Halssiaapa. Our findings underscore the importance of fieldwork timing and the use of multi-temporal and hyperspectral data in detecting vegetation in spatially heterogeneous landscapes.

ARTICLE HISTORY
Received 23 June 2022
Accepted 20 November 2022

KEYWORDS
Hyperspectral remote sensing; peatlands; plant communities; plant functional types; above-ground biomass; leaf area index; field spectroscopy

1 Introduction

Northern peatlands play a large role in global carbon circulation (Loisel and Yu 2013; Rastogi et al. 2019). Their carbon dynamics are linked to vegetation pattern and composition, such as the two-dimensional (2D, the projected) %-cover, above-ground biomass (AGB) and leaf area index (LAI) of plant functional types (PFTs) (Robroek et al. 2015; Lopatin et al. 2019; Rupp et al. 2019; Whitaker et al. 2021; Laine, Korrensalo, and Tuittila 2022). The 2D %-cover of different plant taxa or communities is the most straightforward and most often mapped vegetation parameter with remote sensing. In ecosystem studies, other parameters are also needed. The AGB, a metric for characterizing vegetation productivity and carbon accumulation, is defined as the total standing dry mass of living plants (Graf and Rochefort 2009; Berner et al. 2018). LAI describes the plant canopy structure and is closely related to photosynthesis capacity and energy balance (Chen et al. 1997; Juutinen et al. 2017). On the landscape scale, the ecosystem carbon balance is a vegetation community-specific phenomenon and is connected to the composition of plant communities (Räsänen et al. 2021) and other environmental properties, such as temperature and wetness (Jonsson and Wardle 2010; Strilesky and Humphreys 2012; Robroek et al. 2015).

Peatlands are structurally heterogeneous, having different plant community clusters (PCCs) and fine-scale microtopography. For example, a northern boreal fen can consist of several different plant communities: wet flarks dominated by sedges and wet brown mosses are found in the low-lying positions, lawns dominated by *Sphagnum*, some sedges and forbs in slightly more elevated locations, and in the most elevated locations, there are strings and hummocks

CONTACT Yuwen Pang yuwen.pang@helsinki.fi
Supplemental data for this article can be accessed online at https://doi.org/10.1080/15481603.2022.2152303

with bog-type shrub-dominated vegetation communities (Heiskanen et al. 2021). Previous studies have suggested that in northern peatlands the use of ultra-high spatial resolution (< 0.5 m) and hyperspectral data increase the detectability of vegetation patterns (Räsänen and Virtanen 2019; Räsänen et al. 2020b). Hyperspectral remote sensing gives possibilities to differentiate or predict PCCs and PFTs (Schaepman-Strub et al. 2009; Kattenborn et al. 2019; McPartland et al. 2019) and allows the estimation of plant biophysical metrics, such as AGB and LAI (Chasmer et al. 2020). As examples of hyperspectral studies, Schmidtlein (2004); Schmidtlein (2005) mapped vegetation gradients and Ellenberg indicator values, Middleton et al. (2012) classified four peatland biotopes, Schmidtlein et al. (2012); Harris, Charnock, and Lucas (2015) detected structure of PCCs, and Schweiger et al. (2017) predicted PFTs and traits of PCCs in peatlands. Drone hyperspectral data has been used, for instance, by Räsänen et al. (2020b), who mapped peatland vegetation AGB and LAI. Field or simulated spectroscopy has been used, for example, by Schaepman-Strub et al. (2009), who estimated the fractional cover and AGB of three peatland PFTs, Kattenborn et al. (2019), who distinguished functional types and traits, and McPartland et al. (2019), who characterized peatland PCCs.

The seasonal development of vegetation is one of the main drivers of carbon dynamics in northern ecosystems, and it varies between AGB, LAI and different PFTs (Juutinen et al. 2017; Peichl et al., 2018). Several studies have examined the optimal temporal window for discriminating PCCs, such as Cole, McMorrow, and Evans (2014) within an upland peatland and Beamish et al. (2017) in tundra. Others, like Erudel et al. (2017) and Arroyo-Mora et al. (2018), have investigated the ability to detect vegetation by using seasonal spectra in peatlands but only in the early part of the vegetation growing season, from April to June. Several studies have indicated that multi-temporal spectral data boost vegetation detection performance (Dudley et al. 2015; Vuolo et al. 2018), although the optimal temporal window and the benefits of multi-temporal *in situ* spectroscopy data have rarely been explored (Vuolo et al. 2018; Cai et al. 2020; Bourgeau-Chavez et al. 2021).

In addition to the temporal issues, the spectral resolution also affects the success of spectral identification. Ustin and Middleton (2021) stated in their recent review that high spectral resolution characterized by a narrow bandwidth of 10 nm would be sufficient to identify and quantify plant and ecosystem properties, and other studies have gained acceptable results even with coarser spectral resolution (Chasmer et al. 2020). On the other hand, in Arctic tundra, Davidson et al. (2016) have shown that multispectral satellite data is not able to discriminate and map dominant PCCs, therefore highlighting the need to use hyperspectral data, and Thomson et al. (2021) have found that eight common Arctic plant species could be well distinguished with field spectroscopy and drone multispectral data but not with Sentinel-2 data. Melville et al. (2018), and other examples (Berhane et al. 2018; Bradter et al. 2020), have reported that broadband spectra are able to achieve acceptable classification accuracy for lowland grassland communities; and the accuracy of multispectral data was similar to that of hyperspectral data when monitoring Antarctic vegetation (Turner et al. 2019). Thus, the optimal spectral resolution varies between study areas, ecosystems and analyzed vegetation characteristics, but there have been few studies in peatlands analyzing the optimal spectral resolution.

This study assesses how well peatland vegetation characteristics (PCCs and the 2D %-cover, AGB and LAI of PFTs) can be detected with time-series field spectroscopy data and addresses the following specific questions: (1) What is the optimal temporal window for spectroscopy data acquisition? (2) Does multi-temporal whole-season spectroscopy data add regression model accuracy in vegetation pattern detection? and (3) What is the optimal spectral bandwidth and sampling interval, and how do the results differ when simulated multispectral S2 data is used?

2 Materials and methods

2.1 Study areas

Our study areas were two fens located in the boreal vegetation zone 125 km apart from each other (Figure 1) and with distinctive vegetation and microtopography patterns. Although earlier studies of vegetation, remote sensing and, in particular, carbon exchange in these areas have been carried out (Haapala et al. 2009; Drewer et al. 2010; Li et al. 2016; Räsänen et al. 2020b, 2021), none of the studies has used field spectroscopy data to detect vegetation characteristics in these peatlands.

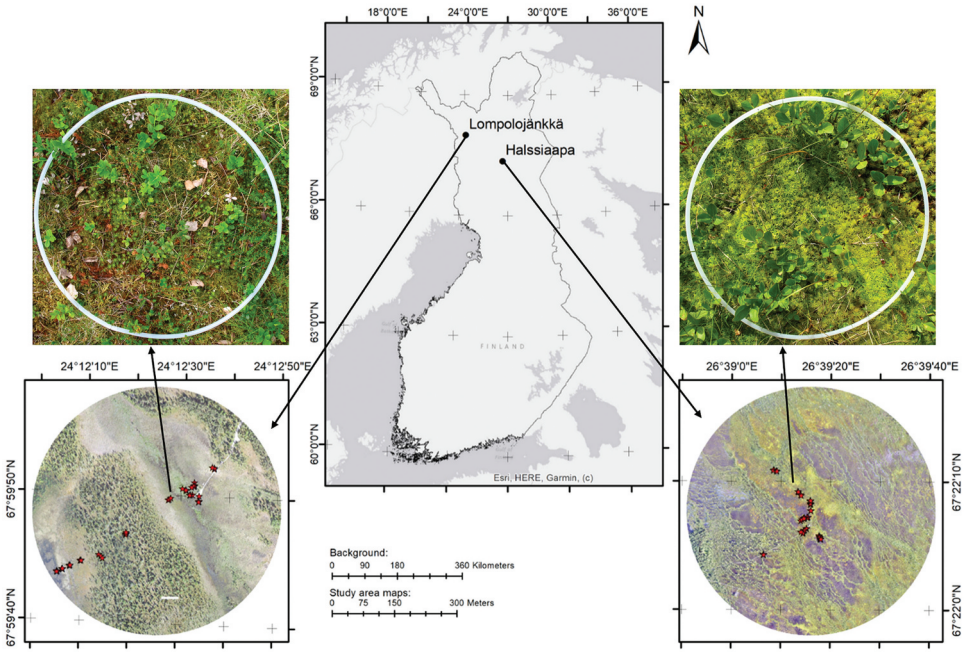

Figure 1. Location of study sites. One example of study plots in both peatlands, and true-color drone images where field inventory plots are marked by red star points. Drone images were captured in July 2018 and 2016 in Lompolojänkkä and Halssiaapa, respectively.

The Lompolojänkkä fen (67° 59.835′ N 24° 12.546′ E, 270 m a.s.l., Figure 1) in Pallas has a flat land surface with major microforms being flarks and lawns (Räsänen et al. 2020a; Zhang et al., 2020). A small stream runs through the fen from south to north. The riparian areas are covered especially with willow shrubs (e.g. *Salix lapponum*) of approximately 60 cm in height. In the central area, a relatively dense vegetation field layer is dominated by *Menyanthes trifoliata, Carex lasiocarpa* and *Carex rostrata*, accompanied by *Sphagnum* and wet brown mosses in the ground layer. The margins and transition area between the fen and adjacent forests include hummocks that are oligotrophic and covered by evergreen shrubs and *Sphagnum* spp. (Aurela et al. 2015). There are no trees in the central area of the peatland, but a few scattered pines with areal crown cover ≤ 10% are found in the peatland margins. Additionally, the study area included six plots from the adjacent forests on mineral and peat soils.

The Halssiaapa fen (67° 22.11′ N 26° 39.27′ E; 180 m a.s.l., Figure 1) in Sodankylä has fine-scale microform patterns, comprising flarks, lawns and strings. The wet surfaces (flarks) are dominated by wet brown mosses, and some vascular plants, *Eriophorum* species, *Scheuchzeria palustris* and *M. trifoliata* are found (Haapala et al. 2009; Morsky et al. 2012). The lawns are located in drier parts between flarks and strings and are dominated by different *Carex* spp. and *Sphagnum* species, such as *Sphagnum lindbergii*. The strings are narrow (1–5 m wide), interconnected ridges covered by shrubs (e.g. *Betula nana, Andromeda polifolia* and *Vaccinium oxycoccos*). Additionally, there is a ≤ 10% crown cover of 5–7 m tall trees, consisting of birches (*Betula pubescens s.l.*) and some pines (*Pinus sylvestris*) (Räsänen et al. 2020a) in the strings that cover approximately 20% of the fen area.

2.2 Field vegetation inventories and ecological analysis

The field inventory was carried out from late May to August 2019 (Table 1). Based on measurements of the nearest Finnish meteorological stations, temperature and precipitation conditions in 2019 were generally close to the average values for the period 2008–2021 at both sites. However, the precipitation levels in July 2019 were less than half of the averages of the reference period (Table S1 in the supplementary material). There were some measurement days in June and August with marked precipitation events preceding the measurements (Table 1), but photographs taken in those measurement days do not show any obvious flooding which could have impacted to our spectral measurements.

Table 1. Schedule of vegetation field inventory and spectroscopy collection.

Site	Date (2019)	Vegetation growing season	No. of spectral plot	Precipitation during previous 5 days (mm)
Lompolojänkkä,	28/05	Early season	36	9.9
39 vegetation plots, 48 plant species	12/06	Early season	38	27.2
	28/06	Early season	36	6.2
	09/07	Mid-season	39	8.2
	24/07	Mid-season	35	5.2
	06/08	Late season	39	0.5
	20/08	Late season	39	39.4
Halssiaapa,	30/05	Early season	42	14.7
43 vegetation plots, 37 plant species	13/06	Early season	42	24.5
	27/06	Early season	43	5.7
	15/07	Mid-season	43	1.4
	26/07	Mid-season	43	0
	08/08	Late season	43	0.8

We sampled 39 and 43 plots with a 50 cm diameter to cover all main plant communities and identified 48 and 37 plant species (see plant species lists in Table S2) in Lompolojänkkä and Halssiaapa, respectively. Plots were located near boardwalks, allowing access to these plots also in wet conditions. For the comparative analysis across PCCs, we sampled three repeat plots near each other that had similar environmental conditions.

In the field, we visually estimated the three-dimensional (3D, each layer estimated separately, summing up to ≥ 100%) and two-dimensional (2D, the projected coverage when looking directly down, summing up to 100%) %-cover of each identified plant species. For shrubs, we further divided the 3D %-cover into green (the photosynthesizing part) and brown (the woody part) proportions during the survey. We also measured the height of vascular plants with a ruler and gave the mean value for each species. We categorized the species into seven PFTs, including deciduous shrubs, evergreen shrubs, forbs, graminoids, wet brown mosses, feather mosses, and *Sphagnum* (see details in Table S2), a PFT division slightly adapted from previous studies by Räsänen et al. (2020a) and Berner et al. (2018). To calculate AGB for vascular plants and mosses and LAI for vascular plants, we adopted empirical relationships based on harvested samples and measured AGB and LAI (given in Table S3) from earlier studies (Räsänen et al. 2020b, 2021). The overall seasonal variation of PFT-specific 2D %-cover, ABG and LAI at each study sites was presented in Figure S1 in the supplementary material.

We utilized the 2D %-cover data to extract the PCCs. Several studies confirmed that fuzzy c-means (FCM) clustering (Bezdek, Ehrlich, and Full 1984) provides a suitable framework for plant community delineation (De Caceres, Font, and Oliva 2010a; Bai and Zhang 2018). It has also been discussed that fuzzy cluster membership values, which range between 0 and 1 and quantify the probability of belonging to certain PCCs, represent ecological gradients more realistically than crisp PCCs (Harris, Charnock, and Lucas 2015; Räsänen et al. 2019). To recognize the PCCs, we firstly used the peak season vegetation inventories that were made in vegetation peak growing seasons as plant species was mostly visible, i.e. around the 20th of July, to conduct Wisconsin double standardization and square-root transformation (Oksanen et al. 2007) and calculate Bray–Curtis (BC) distances via vegan 2.5–7 (Oksanen et al. 2020), which were used to measure the dissimilarity between plots (Ricotta and Podani 2017). Secondly, with the package of cluster 2.1.1 (Maechler et al. 2022), we applied the non-metric multidimensional scaling algorithm to the BC matrix by executing 20 random starts to ensure a scaling stress value below 0.1 and restricted the community characteristics to four ordination axes. Thirdly, we searched for the optimum cluster number between 1 and 10 by maximizing the silhouette width (Campello and Hruschka 2006) and then applied the optimal cluster number to FCM clustering with a membership exponent of 1.5 (Maechler et al. 2022). Finally, for each plot, we yielded the cluster membership value. To find out the representative species of identified PCCs, we used an extension of the original indicator value method (De Caceres, Legendre, and Moretti 2010b) with 999 random permutations by using the package of indicspecies 1.7.9 (De Caceres, Jansen, and De Caceres 2020). The analyses were implemented in the two study areas separately using R (Team 2020) packages.

2.3 Spectroscopy data collection, processing and analysis

We carried out field spectral reflectance measurements concurrently with vegetation measurements (Table 1)

with an Analytical Spectral Devices Handheld II spectroradiometer (Analytical Spectral Devices, Boulder, CO, USA), which assembles a wavelength range of 325 to 1075 nm with a 1 nm interval and 3 nm bandwidth. Before measuring the actual plots, we optimized the integration time for illumination conditions and measured the Labsphere Spectralon white reference panel (assumed to have 100% reflectance), which was kept level on a maximum distance of 10 cm. When measuring the reflectance in the plots, we positioned the spectroradiometer 1 m above the land surface to cover the circular plot with a diameter of 50 cm (field of view 25°). We held the spectroradiometer in hand and pointed it directly down, checked by the laser pointer. We conducted the measurements with an arm out to the side reducing the reflection interference and avoided standing in front of the sun so that we did not shade the plot. We calibrated the device approximately every 5 minutes or when illumination conditions changed, including optimization and measurement of the white reference panel. For each plot, we recorded three scans at one time. In total, we collected 786 and 768 spectral records in Lompolojänkkä and Halssiaapa, respectively (Table 1).

Before spectral preprocessing, the spectral data were transferred into reflectance on the software of ASD ViewSpec Pro, where the small discrepancies of assuming the 100% reflecting of reflectance panel were accounted for. We visually interpreted the three scans of each measurement to select the best one (Figure S2). If three scans were similar, the midmost one was chosen. If there was an obvious increase or decrease in lightning conditions, we selected the one which was taken immediately after the calibration. This latter criterion was used for 6% and 2% of the measurements in Lompolojänkkä and Halssiaapa, respectively.

Due to a small signal-to-noise ratio resulting from the systematic effect of the spectroradiometer and strong atmospheric absorption mainly resulting from the presence of water vapor (Erudel et al. 2017), we removed spectral bands from 350 to 400 nm and 901 to 1050 nm and used only the wavelength region between 400 and 900 nm in the analyses. Based on our data, the reflectance of vegetation ranged from 0.1 to 0.4, while the value dropped to below 0.1 when there was high surface water content, such as in the flark PCC. Besides spectral signature transformation measures, spectral normalization has been utilized to remove wavelength-independent magnitude differences between spectra and enhance wavelength-dependent effects (Siegmann et al. 2014; Philpot, Jacquemoud, and Tian 2021), which therefore allows spectral comparison across sites and over seasons. A study by Cao et al. (2017) suggested that the normalization of spectra facilitated hyperspectral classification. To this end, we calculated the normalized spectra with the following equation:

$$Rn(\lambda) = \frac{\mathrm{R}(\lambda)}{\mathrm{Max}(\mathrm{R})} \tag{1}$$

where λ is the wavelength ranging from 400 to 900 nm, Rn(λ) is the normalized spectrum, R(λ) is the original spectrum, and Max(R) is the maximum reflectance of each original spectrum, independently. After normalization, we smoothed all spectra by using a Savitzky–Golay filter, which has been widely applied to field spectroscopy preprocessing (Zimmermann and Kohler, 2013).

To address the first research question, we used only single-date spectra to predict PCC, AGB and LAI for relevant dates, respectively. Then, to answer the second question, we combined multi-temporal spectral and vegetation data (i.e. the whole season) to construct regressions, which were compared to single-date regressions accordingly. When answering the third research question, we resampled the whole-season field spectroradiometer data with 1 nm sampling interval into four other spectral sampling interval options (i.e. 5, 10, 20 and 50 nm) by averaging the reflectance of the original spectrum in corresponding wavelength regions. We also simulated two types of Sentinel-2A (S2A) band options: 4 bands (blue, green, red and near-infrared, S2A-4) and 8 bands (4-band option and 4 vegetation red-edge bands, S2A-8) (the technical information for spectral resampling and visualized figures is given in Table S4 and Figure S3). This data processing was done with the hsdar package (Lehnert et al. 2019) in R (Team 2020).

The multivariate random forest (MRF) algorithm allows the use of multiple response variables simultaneously and is able to yield a higher predictive rate than the univariate random forest (Segal and Xiao 2011). With the package randomForestSRC 2.11.0 (Ishwaran, Kogalur, and Kogalur 2022) in R (Team 2020), we applied the MRF with 500 trees to establish regressions in which the spectral reflectance composed of the explanatory variables and vegetation characteristics (FCM membership of PCCs and the 2D %-cover,

AGB and LAI of PFTs) were response variables. In the PFT regressions, the following response variables were tested: (1) vascular plants, (2) mosses total, (3) ground-layer vegetation total and (4) seven separate PFTs.

To assess model performance, we calculated three validation parameters, the percentage of variance explained (random forest pseudo R^2 = 1 − (mean square error)/variance(response)), the root mean square error (RMSE) and the normalized RMSE (nRMSE = RMSE/range(response)), with an out-of-bag evaluation in which two-thirds of the data in each tree is used for training and the rest for evaluation. It has been noted in earlier research that there is no need for separate cross-validation or independent test data when using OOB evaluation (Breiman 2003; Canovas-Garcia et al. 2017). To get robust regression results, we repeated the MRF regression 20 times and calculated the mean R^2, RMSE and nRMSE. A flowchart of the materials and methods is presented in Figure 2.

3 Results

3.1 Peatland vegetation community cluster results

The optimal number of PCCs was six in both studied peatlands (Figure 3) by an ordination scale stress of 0.084 in Lompolojänkkä and 0.1023 in Halssiaapa. These PCCs were named based on their vegetation properties and microtopography, resulting in one flark and three lawns at both sites, while two hummocks or strings in Lompolojänkkä or Halssiaapa, respectively. Most of the PCCs were separated well in the analyses, except LawnB and LawnC in Lompolojänkkä seemed to overlap (Figure 3). However, they had different indicator species (Table S5). Additionally, lawn clusters in Lompolojänkkä had different seasonal vegetation development patterns. LawnA had relatively high components of vascular plants and thus clear seasonality, LawnB had a %-cover peak around 20th of

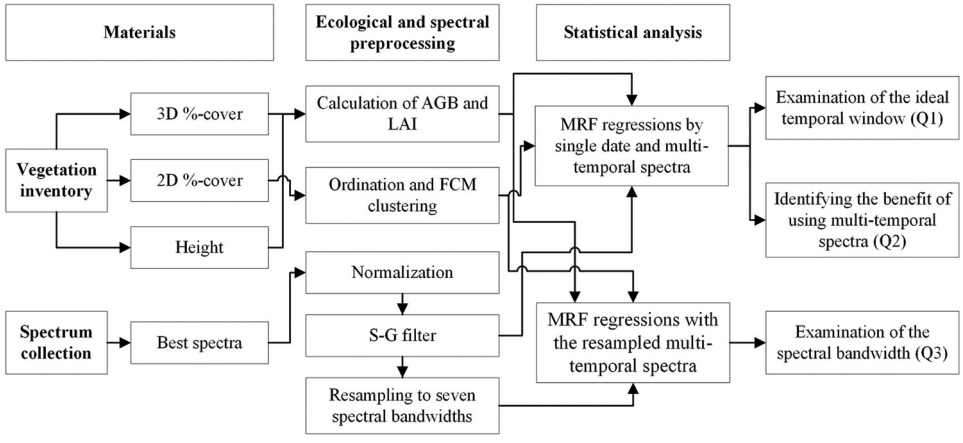

Figure 2. The flowchart of the study. 3D and 2D refer to three- and two-dimensional %-cover, respectively. FCM refers to fuzzy c-means; MRF to the multivariate random forest; Q1, Q2 and Q3 to the research question 1, 2, and 3, respectively.

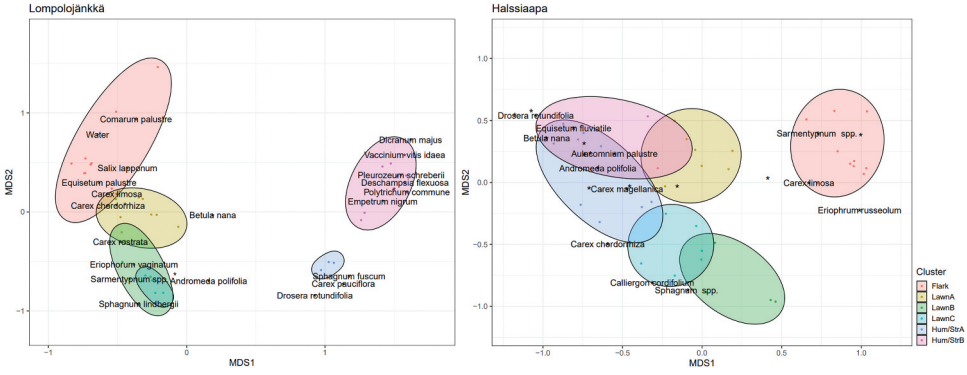

Figure 3. Identified plant community clusters. In the figure, MDS 1 and 2 refer to the first two non-metric dimensional scaling coordinate, and Hum/Str to hummock (Lomplojänkkä) or string (Halssiaapa).

July, while the %-cover of LawnC was mostly stable over seasons (Figure S4).

In general, the reflectance was higher in the visible wavelength region during the early season from May to mid of June (Figure 4). After that, the reflectance dropped, reaching the lowest values around 685 nm by late July. In the near-infrared region, between 700 and 900 nm, opposite temporal progress is observed, with the lowest values typically taking place during early summer and increasing after that as vegetation increases. Seasonal variation also clearly differed between PCCs (Figure 4).

3.2 Seasonal differences in spectral regressions

3.2.1 Plant community clusters

For the whole-season spectral regressions of PCCs, the average R^2 was 48.0% (RMSE 0.188, Table S6) and 42.6% (RMSE 0.155, Table S6) in Lompolojänkkä and Halssiaapa, respectively (Figure 5). Halssiaapa regressions yielded higher explanatory rates in single-date models than in Lompolojänkkä, in particular during late July and August (i.e. peak to late growing season), with R^2 ranging from 33.5% to 39.3% (RMSE 0.160–0.167, Table S6). The whole-season models had considerably higher R^2 when compared with single-date ones, on average by 24.6%-points (RMSE dropped by 0.044, Table S6) and 13.7%-points (RMSE dropped by 0.020, Table S6) at Lompolojänkkä and Halssiaapa, respectively. None of the single-date regression models had as high a regression performance as the whole-season models.

With regard to separate PCCs, the whole-season models mostly improved the explanatory rate compared with single-date ones (Figure 5). However, in

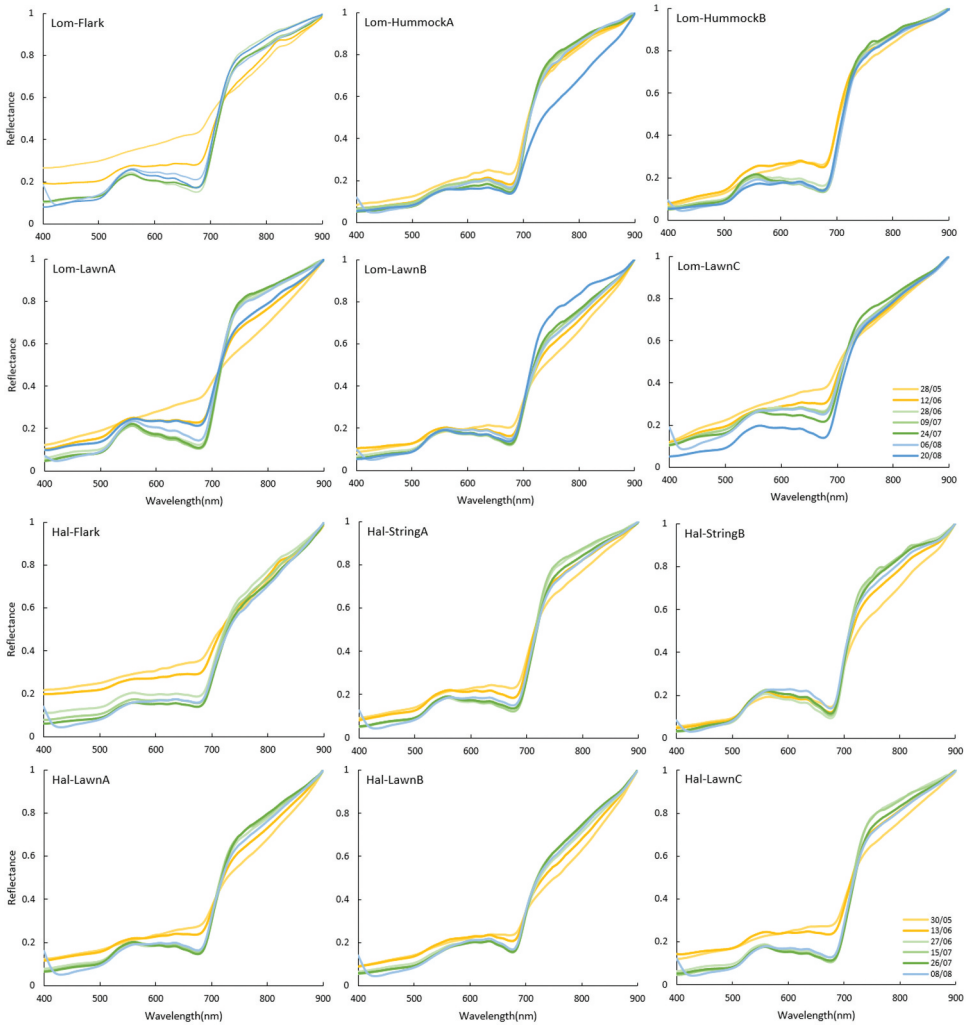

Figure 4. Seasonal normalized spectra of six plant community clusters. Lom and Hal refer to Lompolojänkkä and Halssiaapa, respectively.

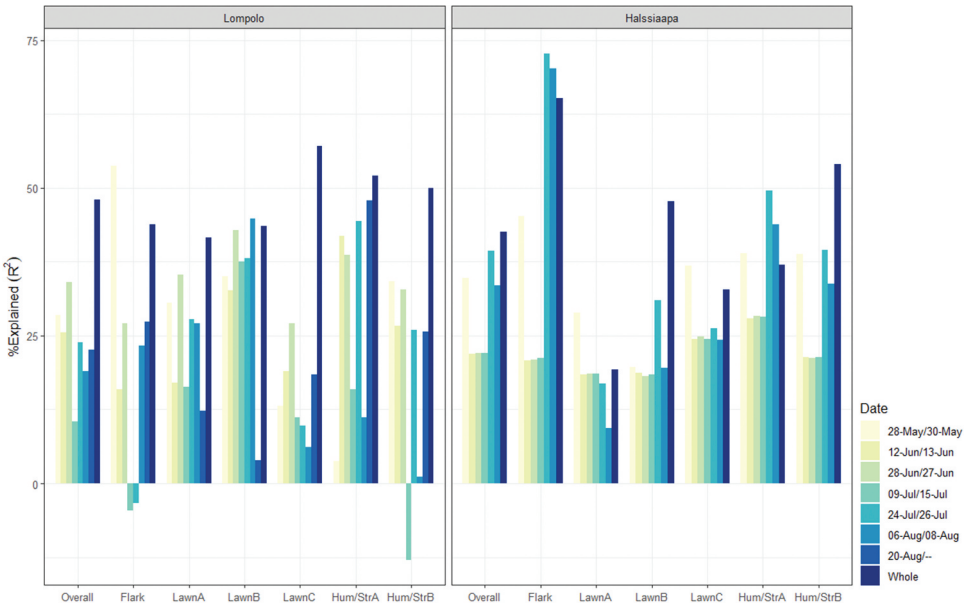

Figure 5. Spectral regression explained rates in terms of overall and specific plant community clusters, in which Hum/Str refers to hummocks or strings. The hummocks exist only in Lompolojänkkä and strings only in Halssiaapa. The descriptions of communities are given in Table S5. In the legend, the former dates are for Lompolojänkkä and the latter ones for Halssiaapa. The root mean square error of regressions is reported in Tables S6 and S7.

certain PCCs, such improvement was not the case. For example, flark had the highest R^2 and lowest RMSE in late May and August in Lompolojänkkä and Halssiaapa, respectively (Figure 5 and Table S7). The PCC-specific explanatory rates of individual date regressions over June to July were stable in Halssiaapa, even though R^2 from these dates was noticeably lower than that reported in the whole-season regressions. However, in Lompolojänkkä, there was a considerable variation in R^2 among single-date models, resulting in a high SD (6.3–17.8%) (Table S6).

3.2.2 Plant functional types

When compared with single-date regression models, the whole-season models improved R^2 by 10.2–32.1%-points, 15–23.7%-points and 23.7–33%-points for %-cover, AGB and LAI, respectively (Figure 6). The 2D %-cover regressions had higher R^2 (53.9–69.1%) than the AGB (43.1–60.5%) and LAI (44.4–51.3%) regressions. In the single-date regressions, early growing season (late May to mid-June) models had the highest explanatory rates for estimating 2D %-cover (excluding the vascular plant total, which got the highest explanatory rates in the late season, i.e. late July and early August) and AGB, while the single-date regressions performed poorly for LAI. Total moss 2D %-cover and AGB were best detected in the early and late seasons when vascular plants were not covering them.

In most cases, the whole-season models had the best explanatory rates, and there were no consistent optimal temporal periods for several PFTs (Figure 6). Nevertheless, for some PFTs, some single-date models had comparable regression performance with the whole-season models, but the optimal temporal window varied between sites. For instance, dates from July to August were optimal for estimating the 2D %-cover of PFTs other than feather mosses and the AGB and LAI of evergreen shrubs in Halssiaapa. In Lompolojänkkä, single-date models for specific PFTs had mostly low regression performance, while the 2D %-cover of deciduous shrubs, feather mosses and *Sphagnum* was best detected in late May to mid-June, and for graminoids, the optimal season was between June and July.

3.3 Impacts of spectral resolution on detectability

3.3.1 Plant community clusters

The best overall model performance was obtained at the sampling interval of 1–20 nm, with an R^2 of 45.1–48.0% (RMSE 0.188–0.193, Table S9) in Lompolojänkkä and 42.6–44.1% (RMSE 0.153–0.155, Table S9) in

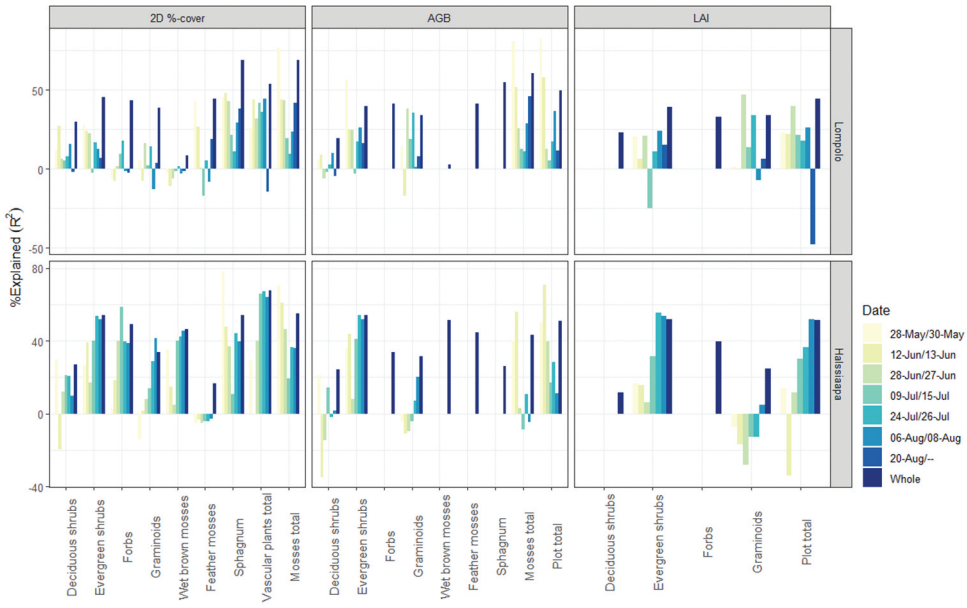

Figure 6. Explained variance (R^2) of two-dimensional (2D) %-cover, above-ground biomass (AGB) and leaf area index (LAI) in terms of various plant functional types by single-date and whole-season models. In the legend, the former dates are for Lompolojänkkä and the latter ones for Halssiaapa. The root mean square error of these regression models is reported in Table S8. Because the AGB or LAI component of several PFTs was not accurately estimated on certain dates, only some specific PFTs were examined by the single-date spectral regression models.

Halssiaapa (Figure 7). With S2A-4, R^2 declined by 9.4 and 9.6%-points from the best models in Lompolojänkkä and Halssiaapa, respectively. Specifically, a clear downward trend in the explanatory rate was found in most PCCs with coarser spectral resolution (Figure 7). In most PCCs, there were small changes in R^2 between 1 and 20 nm, while R^2 was substantially lower for 50 nm and the two S2A options, except for LawnB and HumA in Lompolojänkkä and LawnC in Halssiaapa.

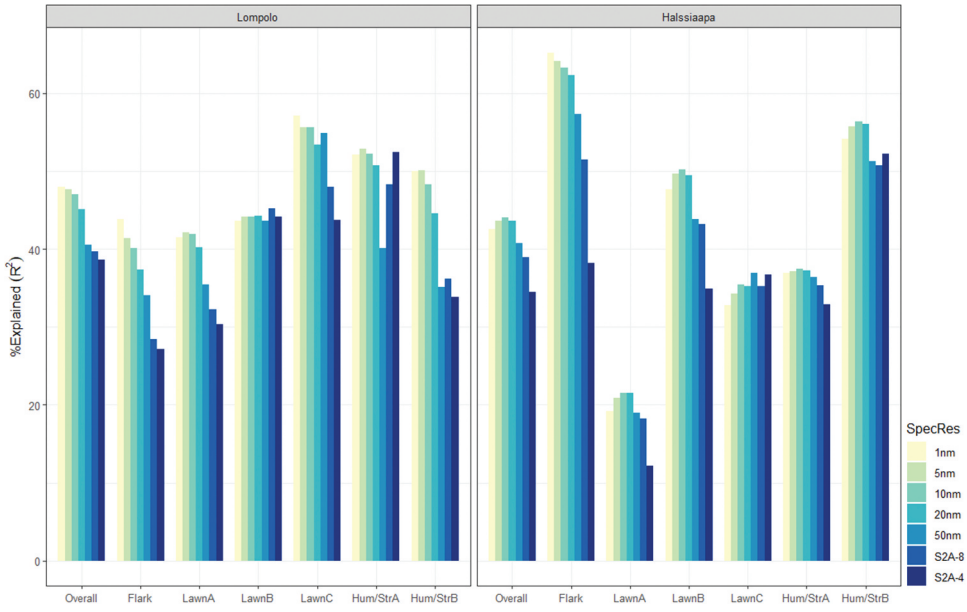

Figure 7. Explained variance (R^2) of spectral regressions in terms of regional overall and specific plant community clusters, in which Hum/Str refers to hummocks or strings. The hummocks only exist in Lompolojänkkä and strings in Halssiaapa. The root mean square error of regressions is reported in Tables S9 and S10. SpecRes = spectral resolution, i.e. the sampling bandwidth; S2A = Sentinel-2A.

3.3.2 Plant functional types

The spectral sampling interval between 1 and 20 nm had the highest regression performance and, particularly for 2D %-cover and AGB, the regression performance decreased considerably with wider sampling interval (Figure 8). For LAI, changing the spectral bandwidth yielded relatively small changes in model performance, with the decrease in R^2 being 1.9 and 6.4%-points in Lompolojänkkä and Halssiaapa, respectively. Also, for separate PFTs, the sampling interval from 1 to 20 nm generated the highest explanatory rates, but for LAI, the differences between intervals were small (Figure 8). For instance, the regression performance of the LAI of forbs exceeded or was close to that of 1 nm-based regressions with all wider spectral bandwidth.

4 Discussion

Our regression analysis results show that we were able to detect vegetation patterns most accurately with the whole-season data and spectral sampling interval below 10–20 nm. In most cases, poor regression performance was reported for single-date models (Figures 5 and 6). These findings are in line with prior research, emphasizing the benefits of multi-temporal data (Langley, Cheshire, and Humes 2001; Dudley et al. 2015; Vuolo et al. 2018; Wakulinska and Marcinkowska-Ochtyra 2020). For instance, Millard et al. (2020) and Rapinel et al. (2020) have shown that using the full growing season remote sensing data achieved higher peatland vegetation detection accuracy than using a subset of a few dates. Moreover, our results exhibited the higher spectral detectability of certain PFTs, in particular *Sphagnum*, followed by shrubs and forbs, agreeing with conclusions in earlier studies (Schaepman-Strub et al. 2009; McPartland et al. 2019; Räsänen et al. 2020a, 2020b). Conversely, graminoids, due to their thin leaves, are known to be difficult to detect (Lopatin et al. 2017; McPartland et al. 2019; Räsänen et al. 2020b).

Some studies have shown that the best discrimination of PCCs occurs when plant species have their maximum canopy during the seasonal peak season (Beamish et al. 2017; Arroyo-Mora et al. 2018; Palace et al. 2018). However, our results do not fully support this finding (Figure 5). In particular, the poor regression accuracy was found in flark and hummcokB in Lompolojänkkä during June-July. Instead, we suggest that for certain PCCs, such as flarks and hummocks/strings, May to mid-June (the early growing season) and July to August (the peak season) are the most appropriate periods for vegetation detection in Lompolojänkkä and Halssiaapa, respectively (Figure

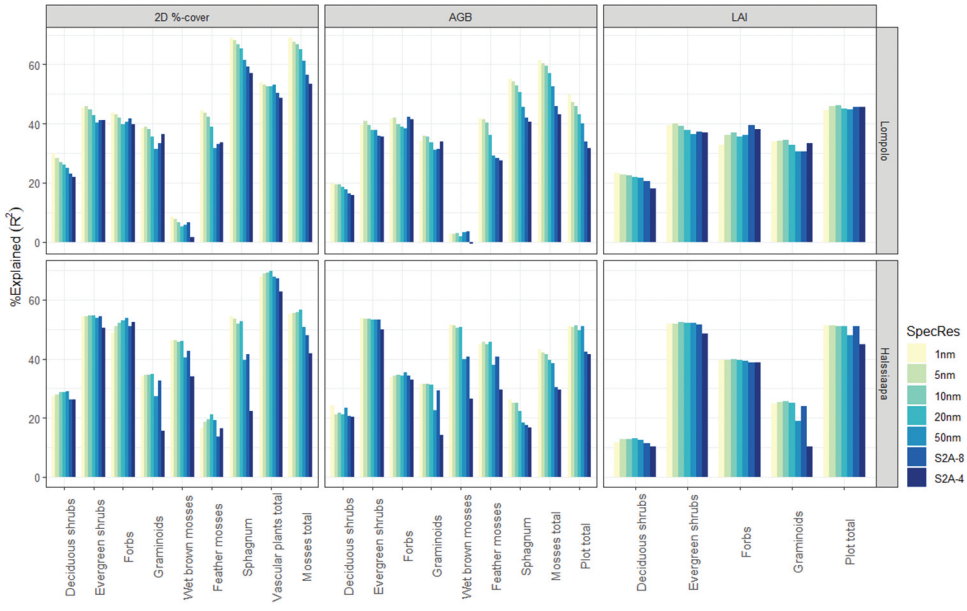

Figure 8. Explained variance (R^2) of two-dimensional (2D) %-cover, above-ground biomass (AGB) and leaf area index (LAI) in terms of various plant functional types. The root mean square error of these regression models is reported in Table S11. SpecRes = spectral resolution, i.e. the sampling interval; S2A = Sentinel-2A.

5). This could be due to differences in the plant composition, the phenological development of dominating PFTs (Dudley et al. 2015), and how these PFTs are layered in relation to each other by PCCs. For instance, in Lompolojänkkä, there was larger %-cover of water in flarks and less wet brown mosses than in Halssiaapa, and higher coverage of graminoids, and high %-cover of *Sphagnum* or wet brown mosses in hummocks below vascular plants. Additionally, a rapid variation of %-cover of the vascular plant was found in these two PCCs during July (Figure S4), possibly causing a large variation in the observability of PCCs during certain dates.

Some PFTs could not be predicted well at all; especially in some single date models, AGB of deciduous shrubs and graminoids had low regression performance at both sites on certain dates (Figure 6). That is possibly caused by several reasons. Some PFTs are common only in certain PCCs (Figure S4). For instance, there is a high proportion of deciduous shrubs LawnA, while it is quite low in other PCCs. As for mosses, they were poorly predicted in single-date spectral regressions; in particular the wet brown mosses got rather poor predictions accurancy in Lompolojänkkä (Figure 6). This is understandable, as the wet brown mosses are covering only small part in Lompolojänkkä, but their %-cover is much higher in Halssiaapa (Figure S1). Additionally, in Halssiaapa, there is less vegetation above the wet brown mosses, especially in flarks (Figure S4), thus yielding a higher R^2. In addition, PFTs with deciduous leaves are obviously not well detected in the early season when they have not yet fully developed. This also makes some other PFTs easier to detect in early vegetation growing seasons, like *Sphagnum* and other mosses growing below the deciduous vascular plants (Figure 5). The impact of wilting graminoids and deciduous shrubs and litter fall can be also considerable in some PCCs. There are differences in several seasonal development patterns PFTs, including leaf structure and foliar chemistry, impacting the possibility of distinguishing between evergreen vs deciduous and high-growing vs low-growing PFTs (Kattenborn et al. 2019). However, in most cases, the modeling accuracy of single-date regressions varied widely; thus, no appropriate temporal window was found.

From a spectral resolution perspective, our results indicate that extremely high spectral resolution data, i.e. spectral sampling interval < 20 nm, is not necessarily needed to detect plant properties (Figures 7 and 8). This result is in line with previous studies, which have emphasized the benefits of hyperspectral data in identifying specific absorption and reflection bands indicative of plant biophysics and identification of individual species (McPartland et al. 2019; Bradter et al. 2020; Oldeland et al., 2021), while some, such as Belluco et al. (2006); Pang et al. (2020), have noted that part of the spectral bands may be redundant. To this end, in the last decade, more researchers have shown that Sentinel-2 has sufficient spectral resolution to explore vegetation characteristics (Arroyo-Mora et al. 2018; Bradter et al. 2020; Wakulinska and Marcinkowska-Ochtyra 2020). Our results only partially support this, since S2A yielded relatively high accuracies in some cases, such as in the detection of *Sphagnum* lawns (LawnB in Lompolojänkkä and LawnC in Halssiaapa, Figure 7) and estimation of four vascular PFTs (Figure 8), but lower accuracies in other cases.

It has been found in several studies that, in general, the 2D %-cover is easier to estimate than AGB and LAI (McPartland et al. 2019; Räsänen et al. 2020a, 2020b), and their explained rates vary among PCCs and PFTs (Bratsch et al. 2016, 2017; Kattenborn et al. 2019). The ability to predict different plant properties depends on how unique their spectral signal is but also how common they are in the landscape, and AGB and LAI detection depends also on how vegetation PFTs are layered. Moreover, canopies with a high LAI reflect more than canopies with a medium or low LAI. However, in peatlands, a high frequency of flooding and bare/peat ground occurs in several PCCs (i.e. hollows and flarks), and LAI was estimated only for vascular plants, which weakened the PFT-specified LAI derivation with the loss of high spectral resolution (Darvishzadeh et al. 2008; Adam, Mutanga, and Rugege 2010).

In addition, in our analyses, we used only ultra-high spatial resolution field spectroscopy data collected 1 m above the ground, covering only about 0.15 m^2 per plot, and no actual aerial or satellite-based data. During the last two decades, the field spectroradiometer has played a vital role in characterizing the reflectance of vegetation patterns and providing an approach to upscale measurement at both the field (canopy and leaves) and laboratory levels (Bratsch et al. 2016; Davidson et al. 2016; Melville et al., 2018; Pang et al. 2020; Yeo et al., 2020; Thomson et al. 2021) but, in any case, some care is needed when

interpreting the results and applying them in studies based on remotely sensed data.

Generally, the more detailed the aim of the classification (i.e. the more PCCs or land cover classes), the less accurate it is (Räsänen and Virtanen 2019). In line with previous studies (e.g. (Rapinel et al. 2019; Wakulinska and Marcinkowska-Ochtyra 2020)), we got a relatively high R^2 for PCC regressions by multi-temporal S2A options (Figure 7). This suggests that multi-temporal satellite data could yield higher accuracy than a single date data. Nevertheless, when modeling biomass and LAI, our results were approximately on par with an earlier study using hyperspectral drone imagery in Halssiaapa (Räsänen et al. 2020b). To understand these issues better, future studies should examine how the results differ when multi-temporal hyperspectral data is collected from drones or manned aircrafts. Also, higher regression accuracy was gained in moss-dominated PCCs, the relatively high R^2 in lawns (LawnB and LawnC in both sites that are mostly dominated by *Sphagnum*, see Table S4 for details) and flarks (Figure 5), which followed other results which reported that the *Sphagnum* spp. type (Erudel et al. 2017; McPartland et al. 2019) and mossy tussock tundra (Bratsch et al. 2016) prediction models had high accuracy.

5 Conclusion

We compared the influence of temporal and spectral resolution on peatland vegetation pattern detection by using field spectroscopy data for two northern peatlands. Our results emphasized that the multi-temporal and high spectral resolution data increased model performance when compared with single-date data and coarser spectral resolution. Moreover, our results suggested that there is no single optimal temporal window but that the optimal timing varies between sites and studied vegetation characteristics. Based on these findings, we propose that future research utilizing drone or satellite data should use multi-temporal data. Otherwise, the peak-season data should be used if all PFTs or overall cover, AGB or LAI are of interest, but for mosses, early-season data probably functions better. Finally, the optimal spectral sampling interval seems at 1 to 20 nm per band.

Acknowledgements

YP acknowledges the support of the China Scholarship Council for her PhD research (Grant no. 202008330336) at the University of Helsinki. Field data collection was funded by the Academy of Finland (Grant no. 30851). We also acknowledge the editor and the anonymous reviewers for their insightful comments, which helped us to significantly improve our manuscript.

Disclosure statement

No potential conflict of interest was reported by the author(s).

Funding

This work was supported by the China Scholarship Council [202008330336]; Academy of Finland [30851].

ORCID

Yuwen Pang http://orcid.org/0000-0002-0478-1225

Data availability

The data that support the findings of this study are available at https://zenodo.org/record/7350306#.Y4Sen3ZBxaQ.

References

Adam, E., O. Mutanga, and D. Rugege. 2010. "Multispectral and Hyperspectral Remote Sensing for Identification and Mapping of Wetland Vegetation: A Review." *Wetlands Ecology and Management* 18 (3): 281–296. doi:10.1007/s11273-009-9169-z.

Arroyo-Mora, J. P., M. Kalacska, R. Soffer, G. Ifimov, G. Leblanc, E. S. Schaaf, and O. Lucanus. 2018. "Evaluation of Phenospectral Dynamics with Sentinel-2A Using a bottom-up Approach in a Northern Ombrotrophic Peatland." *Remote Sensing of Environment* 216: 544–560. doi:10.1016/j.rse.2018.07.021.

Aurela, M., A. Lohila, J. P. Tuovinen, J. Hatakka, T. Penttila, and T. Laurila (2015). Carbon Dioxide and Energy Flux Measurements in Four northern-boreal Ecosystems at Pallas. *Boreal Environment Research*, 20(4), 455–473. Retrieved from <Go>://WOS:000361411500002

Bai, X. H., and J. T. Zhang. 2018. "Environmental Interpretation of Forest Communities in Xiaowutai Mountain by Fuzzy Mathematics Analysis." *Ecological Informatics* 48: 178–186. doi:10.1016/j.ecoinf.2018.09.006.

Beamish, A. L., N. Coops, S. Chabrillat, and B. Heim. 2017. "A Phenological Approach to Spectral Differentiation of Low-Arctic Tundra Vegetation Communities, North Slope,

Alaska." *Remote Sensing* 9 (11): 1200. ARTN 1200. doi:10.3390/rs9111200.

Belluco, E., M. Camuffo, S. Ferrari, L. Modenese, S. Silvestri, A. Marani, and M. Marani. 2006. "Mapping salt-marsh Vegetation by Multispectral and Hyperspectral Remote Sensing." *Remote Sensing of Environment* 105 (1): 54–67. doi:10.1016/j.rse.2006.06.006.

Berhane, T. M., C. R. Lane, Q. S. Wu, B. C. Autrey, O. A. Anenkhonov, V. V. Chepinoga, and H. X. Liu. 2018. "Decision-Tree, Rule-Based, and Random Forest Classification of High-Resolution Multispectral Imagery for Wetland Mapping and Inventory." *Remote Sensing* 10 (4): 580. ARTN 580. doi:10.3390/rs10040580.

Berner, L. T., P. Jantz, K. D. Tape, and S. J. Goetz. 2018. "Tundra Plant above-ground Biomass and Shrub Dominance Mapped across the North Slope of Alaska." *Environmental Research Letters* 13 (3): 035002. ARTN 035002. doi:10.1088/1748-9326/aaaa9a.

Bezdek, J. C., R. Ehrlich, and W. Full. 1984. "FCM: The Fuzzy c-means Clustering Algorithm." *Computers & Geosciences* 10 (2–3): 191–203. doi:10.1016/0098-3004(84)90020-7.

Bourgeau-Chavez, L. L., S. L. Grelik, M. J. Battaglia, D. J. Leisman, R. A. Chimner, J. A. Hribljan, and E. A. Lilleskov (2021). Advances in Amazonian Peatland Discrimination with Multi-Temporal PALSAR Refines Estimates of Peatland Distribution, C Stocks and Deforestation. *Frontiers in Earth Science*, 9. Retrieved from <Go>://WOS:000744466800001 10.3389/feart.2021.676748

Bradter, U., J. O'Connell, W. E. Kunin, C. W. H. Boffey, R. J. Ellis, and T. G. Benton. 2020. "Classifying grass-dominated Habitats from Remotely Sensed Data: The Influence of Spectral Resolution, Acquisition Time and the Vegetation Classification System on Accuracy and Thematic Resolution." *Science of the Total Environment* 711: ARTN 134584. 10.1016/j.scitotenv.2019.134584.

Bratsch, S. N., H. E. Epstein, M. Buchhorn, and D. A. Walker. 2016. "Differentiating among Four Arctic Tundra Plant Communities at Ivotuk, Alaska Using Field Spectroscopy." *Remote Sensing* 8 (1): 51. ARTN51. doi:10.3390/rs8010051.

Bratsch, S., H. Epstein, M. Buchhorn, D. Walker, and H. Landes. 2017. "Relationships between Hyperspectral Data and Components of Vegetation Biomass in Low Arctic Tundra Communities at Ivotuk, Alaska." *Environmental Research Letters* 12 (2): 025003. ARTN 025003. doi:10.1088/1748-9326/aa572e.

Breiman, L. (2003). Manual for Setting Up, Using, and Understanding Random Forest V4. 0. Retrieved from https://www.stat.berkeley.edu/~breiman/Using_random_forests_v4.0.pdf

Cai, Y. T., X. Y. Li, M. Zhang, and H. Lin. 2020. "Mapping Wetland Using the object-based Stacked Generalization Method Based on multi-temporal Optical and SAR Data." ARTN 102164. 92: 102164. 10.1016/j.jag.2020.102164

Campello, R. J. G. B., and E. R. Hruschka. 2006. "A Fuzzy Extension of the Silhouette Width Criterion for Cluster Analysis." *Fuzzy Sets and Systems* 157 (21): 2858–2875. doi:10.1016/j.fss.2006.07.006.

Canovas-Garcia, F., F. Alonso-Sarria, F. Gomariz-Castillo, and F. Onate-Valdivieso. 2017. "Modification of the Random Forest Algorithm to Avoid Statistical Dependence Problems When Classifying Remote Sensing Imagery." *Computers & Geosciences* 103: 1–11. doi:10.1016/j.cageo.2017.02.012.

Cao, F., Z. Yang, J. Ren, M. Jiang, and W.-K. Ling. 2017. Does Normalization Methods Play a Role for Hyperspectral Image Classification? *arXiv preprint arXiv:1710.02939*.

Chasmer, L., D. Cobbaert, C. Mahoney, K. Millard, D. Peters, K. Devito, . . . B. Brisco. 2020. "Remote Sensing of Boreal Wetlands 1: Data Use for Policy and Management." *Remote Sensing* 12 (8): 1320. ARTN 1320. doi:10.3390/rs12081320.

Chen, J. M., P. M. Rich, S. T. Gower, J. M. Norman, and S. Plummer. 1997. "Leaf Area Index of Boreal Forests: Theory, Techniques, and Measurements." *Journal of Geophysical Research: Atmospheres* 102 (D24): 29429–29443. doi:10.1029/97jd01107.

Cole, B., J. McMorrow, and M. Evans. 2014. "Spectral Monitoring of Moorland Plant Phenology to Identify a Temporal Window for Hyperspectral Remote Sensing of Peatland." *Isprs Journal of Photogrammetry and Remote Sensing* 90: 49–58. doi:10.1016/j.isprsjprs.2014.01.010.

Darvishzadeh, R., A. Skidmore, C. Atzberger, and S. van Wieren. 2008. "Estimation of Vegetation LAI from Hyperspectral Reflectance Data: Effects of Soil Type and Plant Architecture." *International Journal of Applied Earth Observation and Geoinformation* 10 (3): 358–373. doi:10.1016/j.jag.2008.02.005.

Davidson, S. J., M. J. Santos, V. L. Sloan, J. D. Watts, G. K. Phoenix, W. C. Oechel, and D. Zona. 2016. "Mapping Arctic Tundra Vegetation Communities Using Field Spectroscopy and Multispectral Satellite Data in North Alaska, USA." *Remote Sensing* 8 (12): 978. ARTN 978. doi:10.3390/rs8120978.

De Caceres, M., X. Font, and F. Oliva. 2010a. "The Management of Vegetation Classifications with Fuzzy Clustering." *Journal of Vegetation Science* 21 (6): 1138–1151. doi:10.1111/j.1654-1103.2010.01211.x.

De Caceres, M., F. Jansen, and M. M. De Caceres. 2020. "Package 'Indicspecies.'" *Indicators* 8: 1.

De Caceres, M., P. Legendre, and M. Moretti. 2010b. "Improving Indicator Species Analysis by Combining Groups of Sites." *Oikos* 119 (10): 1674–1684. doi:10.1111/j.1600-0706.2010.18334.x.

Drewer, J., A. Lohila, M. Aurela, T. Laurila, K. Minkkinen, T. Penttila, . . . U. M. Skiba. 2010. "Comparison of Greenhouse Gas Fluxes and Nitrogen Budgets from an Ombotrophic Bog in Scotland and a Minerotrophic Sedge Fen in Finland." *European Journal of Soil Science* 61 (5): 640–650. doi:10.1111/j.1365-2389.2010.01267.x.

Dudley, K. L., P. E. Dennison, K. L. Roth, D. A. Roberts, and A. R. Coates. 2015. "A multi-temporal Spectral Library Approach for Mapping Vegetation Species across Spatial and Temporal Phenological Gradients." *Remote Sensing of Environment* 167: 121–134. doi:10.1016/j.rse.2015.05.004.

Erudel, T., S. Fabre, T. Houet, F. Mazier, and X. Briottet. 2017. "Criteria Comparison for Classifying Peatland Vegetation Types Using in Situ Hyperspectral Measurements." *Remote Sensing* 9 (7): 748. ARTN 748. doi:10.3390/rs9070748.

Graf, M., and L. Rochefort. 2009. "Examining the peat-accumulating Potential of Fen Vegetation in the Context of Fen Restoration of Harvested Peatlands." *Ecoscience* 16 (2): 158–166. doi:10.2980/16-2-3128.

Haapala, J. K., S. K. Morsky, S. Saarnio, R. Rinnan, H. Suokanerva, E. Kyro, J. Silvola, P. J. Martikanen, T. HOLOPAINEN, and J. SILVOLA. 2009. "Carbon Dioxide Balance of a Fen Ecosystem in Northern Finland under Elevated UV-B Radiation." *Global Change Biology* 15 (4): 943–954. doi:10.1111/j.1365-2486.2008.01785.x.

Harris, A., R. Charnock, and R. M. Lucas. 2015. "Hyperspectral Remote Sensing of Peatland Floristic Gradients." *Remote Sensing of Environment* 162: 99–111. doi:10.1016/j.rse.2015.01.029.

Heiskanen, L., J. P. Tuovinen, A. Rasanen, T. Virtanen, S. Juutinen, A. Lohila, . . . M. Aurela. 2021. "Carbon Dioxide and Methane Exchange of a Patterned Subarctic Fen during Two Contrasting Growing Seasons." *Biogeosciences* 18 (3): 873–896. doi:10.5194/bg-18-873-2021.

Ishwaran, H., U. B. Kogalur, and M. U. B. Kogalur. 2022. "Package 'Randomforestsrc.'" *Breast* 6: 1.

Jonsson, M., and D. A. Wardle. 2010. "Structural Equation Modelling Reveals plant-community Drivers of Carbon Storage in Boreal Forest Ecosystems." *Biology Letters* 6 (1): 116–119. doi:10.1098/rsbl.2009.0613.

Juutinen, S., T. Virtanen, V. Kondratyev, T. Laurila, M. Linkosalmi, J. Mikola, M. Aurela, A. Räsänen, J.-P. Tuovinen, and M. Aurela. 2017. "Spatial Variation and Seasonal Dynamics of leaf-area Index in the Arctic tundra-implications for Linking Ground Observations and Satellite Images." *Environmental Research Letters* 12 (9): 095002. ARTN 095002. doi:10.1088/1748-9326/aa7f85.

Kattenborn, T., F. E. Fassnacht, S. Schmidtlein, H. Nagendra, and K. He. 2019. "Differentiating Plant Functional Types Using Reflectance: Which Traits Make the Difference?" *Remote Sensing in Ecology and Conservation* 5 (1): 5–19. doi:10.1002/rse2.86.

Laine, A. M., A. Korrensalo, and E.-S. Tuittila. 2022. "Plant Functional Traits Play the Second Fiddle to Plant Functional Types in Explaining Peatland CO2 and CH4 Gas Exchange." *Science of the Total Environment* 834: 155352. doi:10.1016/j.scitotenv.2022.155352.

Langley, S. K., H. M. Cheshire, and K. S. Humes. 2001. "A Comparison of Single Date and Multitemporal Satellite Image Classifications in A semi-arid Grassland." *Journal of Arid Environments* 49 (2): 401–411. doi:10.1006/jare.2000.0771.

Lehnert, L. W., H. Meyer, W. A. Obermeier, B. Silva, B. Regeling, and J. Bendix. 2019. "Hyperspectral Data Analysis in R: The Hsdar Package." *Journal of Statistical Software* 89 (12). doi:10.18637/jss.v089.i12.

Li, T. T., M. Raivonen, P. Alekseychik, M. Aurela, A. Lohila, X. H. Zheng, . . . W. Zhang. 2016. "Importance of Vegetation Classes in Modeling CH4 Emissions from Boreal and Subarctic Wetlands in Finland." *Science of the Total Environment* 572: 1111–1122. doi:10.1016/j.scitotenv.2016.08.020.

Loisel, J., and Z. C. Yu. 2013. "Surface Vegetation Patterning Controls Carbon Accumulation in Peatlands." *Geophysical Research Letters* 40 (20): 5508–5513. doi:10.1002/grl.50744.

Lopatin, J., F. E. Fassnacht, T. Kattenborn, and S. Schmidtlein. 2017. "Mapping Plant Species in Mixed Grassland Communities Using Close Range Imaging Spectroscopy." *Remote Sensing of Environment* 201: 12–23. doi:10.1016/j.rse.2017.08.031.

Lopatin, J., T. Kattenborn, M. Galleguillos, J. F. Perez-Quezada, and S. Schmidtlein. 2019. "Using Aboveground Vegetation Attributes as Proxies for Mapping Peatland Belowground Carbon Stocks." *Remote Sensing of Environment* 231: ARTN 111217. 10.1016/j.rse.2019.111217.

Maechler, M., P. Rousseeuw, A. Struyf, M. Hubert, K. Hornik, and M. Studer. 2022. cluster: Cluster Analysis Basics and Extensions. R package version 2.1.4. https://CRAN.R-project.org/package=cluster.

McPartland, M. Y., M. J. Falkowski, J. R. Reinhardt, E. S. Kane, R. Kolka, M. R. Turetsky, and R. A. Montgomery. 2019. "Characterizing Boreal Peatland Plant Composition and Species Diversity with Hyperspectral Remote Sensing." *Remote Sensing* 11 (14): 1685. ARTN 1685. doi:10.3390/rs11141685.

Melville, B., A. Lucieer, and J. Aryal. 2018. "Assessing the Impact of Spectral Resolution on Classification of Lowland Native Grassland Communities Based on Field Spectroscopy in Tasmania, Australia." *Remote Sensing* 10 (2): 308. ARTN308. doi:10.3390/rs10020308.

Middleton, M., P. Narhi, H. Arkimaa, E. Hyvonen, V. Kuosmanen, P. Treitz, and R. Sutinen. 2012. "Ordination and Hyperspectral Remote Sensing Approach to Classify Peatland Biotopes along Soil Moisture and Fertility Gradients." *Remote Sensing of Environment* 124: 596–609. doi:10.1016/j.rse.2012.06.010.

Millard, K., P. Kirby, S. Nandlall, A. Behnamian, S. Banks, and F. Pacini. 2020. "Using Growing-Season Time Series Coherence for Improved Peatland Mapping: Comparing the Contributions of Sentinel-1 and RADARSAT-2 Coherence in Full and Partial Time Series." *Remote Sensing* 12 (15): 2465. ARTN 2465. doi:10.3390/rs12152465.

Morsky, S. K., J. K. Haapala, R. Rinnan, S. Saarnio, H. Suokanerva, K. Latola, E. Kyrö, J. Silvola, T. Holopainen, and P. J. Martikainen. 2012. "Minor long-term Effects of ultraviolet-B Radiation on Methane Dynamics of a Subarctic Fen in Northern Finland." *Biogeochemistry* 108 (1–3): 233–243. doi:10.1007/s10533-011-9593-z.

Oksanen, J., F. G. Blanchet, R. Kindt, P. Legendre, P. R. Minchin, R. O'hara, and H. Wagner. 2020. "Package 'Vegan.'" *Community Ecology Package, Version* 2 (9): 1–295.

Oksanen, J., R. Kindt, P. Legendre, B. O'Hara, M. H. H. Stevens, M. J. Oksanen, and M. Suggests. 2007. "The Vegan Package." *Community Ecology Package* 10 (631–637): 719.

Oldeland, J., R. Revermann, J. Luther-Mosebach, T. Buttschardt, and J. R. K. Lehmann. 2021. "New Tools for Old Problems —

Comparing Drone- and field-based Assessments of a Problematic Plant Species." *Environmental Monitoring and Assessment*, 193(2). doi:10.1007/s10661-021-08852-2

Palace, M., C. Herrick, J. DelGreco, D. Finnell, A. J. Garnello, C. McCalley, R. K. McArthur, F. Sullivan, and R. Varner. 2018. "Determining Subarctic Peatland Vegetation Using an Unmanned Aerial System (UAS)." *Remote Sensing* 10 (9): 1498. ARTN 1498. doi:10.3390/rs10091498.

Pang, Y., Y. Huang, Y. Zhou, J. Xu, and Y. Wu. 2020. "Identifying Spectral Features of Characteristics of Sphagnum to Assess the Remote Sensing Potential of Peatlands: A Case Study in China." *Mires and Peat* 26: ARTN 25. 10.19189/MaP.2019.OMB.StA.1834.

Peichl, M., M. Gazovic, I. Vermeij, E. de Goede, O. Sonnentag, J. Limpens, and M. B. Nilsson. 2018. "Peatland Vegetation Composition and Phenology Drive the Seasonal Trajectory of Maximum Gross Primary Production." *Scientific Reports* 8 (1). ARTN 8012. doi:10.1038/s41598-018-26147-4.

Philpot, W., S. Jacquemoud, and J. Tian. 2021. "ND-space: Normalized Difference Spectral Mapping." ARTN 112622. 264: 112622. 10.1016/j.rse.2021.112622

Rapinel, S., C. Mony, L. Lecoq, B. Clement, A. Thomas, and L. Hubert-Moy. 2019. "Evaluation of Sentinel-2 time-series for Mapping Floodplain Grassland Plant Communities." *Remote Sensing of Environment* 223: 115–129. doi:10.1016/j.rse.2019.01.018.

Rapinel, S., C. Rozo, P. Delbosc, D. Arvor, A. Thomas, J.-B. Bouzille, F. Bioret, and L. Hubert-Moy. 2020. "Mapping the Functional Dimension of Vegetation Series in the Mediterranean Region Using Multitemporal MODIS Data." *Giscience & Remote Sensing* 57 (1): 60–73. doi:10.1080/15481603.2019.1662167.

Räsänen, A., M. Aurela, S. Juutinen, T. Kumpula, A. Lohila, T. Penttila, T. Virtanen, N. Horning, and J. Zhang. 2020a. "Detecting Northern Peatland Vegetation Patterns at ultra-high Spatial Resolution." *Remote Sensing in Ecology and Conservation* 6 (4): 457–471. doi:10.1002/rse2.140.

Räsänen, A., S. Juutinen, M. Kalacska, M. Aurela, P. Heikkinen, K. Maenpaa, A. Rimali, and T. Virtanen. 2020b. "Peatland leaf-area Index and Biomass Estimation with ultra-high Resolution Remote Sensing." *Giscience & Remote Sensing* 57 (7): 943–964. doi:10.1080/15481603.2020.1829377.

Räsänen, A., S. Juutinen, E.-S. Tuittila, M. Aurela, T. Virtanen, and D. Rocchini. 2019. "Comparing ultra-high Spatial Resolution remote-sensing Methods in Mapping Peatland Vegetation." *Journal of Vegetation Science* 30 (5): 1016–1026. doi:10.1111/jvs.12769.

Räsänen, A., T. Manninen, M. Korkiakoski, A. Lohila, and T. Virtanen. 2021. "Predicting catchment-scale Methane Fluxes with multi-source Remote Sensing." *Landscape Ecology* 36 (4): 1177–1195. doi:10.1007/s10980-021-01194-x.

Räsänen, A., and T. Virtanen. 2019. "Data and Resolution Requirements in Mapping Vegetation in Spatially Heterogeneous Landscapes." ARTN 11120710. 230: 111207. 10.1016/j.rse.2019.05.026

Rastogi, A., M. Strozecki, H. M. Kalaji, D. Lucow, M. Lamentowicz, and R. Juszczak. 2019. "Impact of Warming and Reduced Precipitation on Photosynthetic and Remote Sensing Properties of Peatland Vegetation." *Environmental and Experimental Botany* 160: 71–80. doi:10.1016/j.envexpbot.2019.01.005.

Ricotta, C., and J. Podani. 2017. "On Some Properties of the Bray-Curtis Dissimilarity and Their Ecological Meaning." *Ecological Complexity* 31: 201–205. doi:10.1016/j.ecocom.2017.07.003.

Robroek, B. J. M., V. E. J. Jassey, M. A. R. Kox, R. L. Berendsen, R. T. E. Mills, L. Cecillon, . . . J. Puissant. 2015. "Peatland Vascular Plant Functional Types Affect Methane Dynamics by Altering Microbial Community Structure." *Journal of Ecology* 103 (4): 925–934. doi:10.1111/1365-2745.12413.

Rupp, D., E. S. Kane, C. Dieleman, J. K. Keller, and M. Turetsky. 2019. "Plant Functional Group Effects on Peat Carbon Cycling in a Boreal Rich Fen." *Biogeochemistry* 144 (3): 305–327. doi:10.1007/s10533-019-00590-5.

Schaepman-Strub, G., J. Limpens, M. Menken, H. M. Bartholomeus, and M. E. Schaepman. 2009. "Towards Spatial Assessment of Carbon Sequestration in Peatlands: Spectroscopy Based Estimation of Fractional Cover of Three Plant Functional Types." *Biogeosciences* 6 (2): 275–284. doi:10.5194/bg-6-275-2009.

Schmidtlein, S. 2004. "Mapping of Continuous Floristic Gradients in Grasslands Using Hyperspectral Imagery." *Remote Sensing of Environment* 92 (1): 126–138. doi:10.1016/j.rse.2004.05.004.

Schmidtlein, S. 2005. "Imaging Spectroscopy as a Tool for Mapping Ellenberg Indicator Values." *Journal of Applied Ecology* 42 (5): 966–974. doi:10.1111/j.1365-2664.2005.01064.x.

Schmidtlein, S., H. Feilhauer, H. Bruelheide, and D. Rocchini. 2012. "Mapping Plant Strategy Types Using Remote Sensing." *Journal of Vegetation Science* 23 (3): 395–405. doi:10.1111/j.1654-1103.2011.01370.x.

Schweiger, A. K., M. Schutz, A. C. Risch, M. Kneubuhler, R. Haller, M. E. Schaepman, and R. Chisholm. 2017. "How to Predict Plant Functional Types Using Imaging Spectroscopy: Linking Vegetation Community Traits, Plant Functional Types and Spectral Response." *Methods in Ecology and Evolution* 8 (1): 86–95. doi:10.1111/2041-210x.12642.

Segal, M., and Y. Y. Xiao. 2011. "Multivariate Random Forests." *WIREs Data Mining and Knowledge Discovery* 1 (1): 80–87. doi:10.1002/widm.12.

Siegmann, B., C. Glasser, S. Itzerott, and C. Neumann. 2014. "An Enhanced Classification Approach Using Hyperspectral Image Data in Combination with in Situ Spectral Measurements for the Mapping of Vegetation Communities." *Photogrammetrie - Fernerkundung - Geoinformation* 2014 (6): 523–533. doi:10.1127/pfg/2014/0243.

Strilesky, S. L., and E. R. Humphreys. 2012. "A Comparison of the Net Ecosystem Exchange of Carbon Dioxide and Evapotranspiration for Treed and Open Portions of A Temperate Peatland." *Agricultural and Forest Meteorology* 153: 45–53. doi:10.1016/j.agrformet.2011.06.006.

R Core Team. 2020. R: A Language and Environment for Statistical Computing. Retrieved from https://www.R-project.org/

Thomson, E. R., M. P. Spiegel, I. H. J. Althuizen, P. Bass, S. L. Chen, A. Chmurzynski, and A. H. Halbritter. 2021. "Multiscale Mapping of Plant Functional Groups and Plant Traits in the High Arctic Using Field Spectroscopy, UAV Imagery and Sentinel-2A Data." *Environmental Research Letters* 16 (5): 055006. ARTN 055006. doi:10.1088/1748-9326/abf464.

Turner, D. J., Z. Malenovsky, A. Lucieer, J. D. Turnbull, and S. A. Robinson. 2019. "Optimizing Spectral and Spatial Resolutions of Unmanned Aerial System Imaging Sensors for Monitoring Antarctic Vegetation." *IEEE Journal of Selected Topics in Applied Earth Observations and Remote Sensing* 12 (10): 3813–3825. doi:10.1109/Jstars.2019.2938544.

Ustin, S. L., and E. M. Middleton. 2021. "Current and near-term Advances in Earth Observation for Ecological Applications." *Ecological Processes* 10(1). ARTN 1. doi:10.1186/s13717-020-00255-4.

Vuolo, F., M. Neuwirth, M. Immitzer, C. Atzberger, and W.-T. Ng. 2018. "How Much Does multi-temporal Sentinel-2 Data Improve Crop Type Classification?" *International Journal of Applied Earth Observation and Geoinformation* 72: 122–130. doi:10.1016/j.jag.2018.06.007.

Wakulinska, M., and A. Marcinkowska-Ochtyra. 2020. "Multi-Temporal Sentinel-2 Data in Classification of Mountain Vegetation." *Remote Sensing* 12 (17): 2696. ARTN 2696. doi:10.3390/rs12172696.

Whitaker, J., H. R. Richardson, N. J. Ostle, A. Armstrong, and S. Waldron. 2021. "Plant Functional Type Indirectly Affects Peatland Carbon Fluxes and Their Sensitivity to Environmental Change." *European Journal of Soil Science* 72 (2): 1042–1053. doi:10.1111/ejss.13048.

Yeo, S., V. Lafon, D. Alard, C. Curti, A. Dehouck, and M.-L. Benot. 2020. "Classification and Mapping of Saltmarsh Vegetation Combining Multispectral Images with Field Data." ARTN 106643. 236: 106643. 10.1016/j.ecss.2020.106643

Zhang, H., E.-S. Tuittila, A. Korrensalo, A. Rasanen, T. Virtanen, M. Aurela, and T. Penttilä. 2020. "Water Flow Controls the Spatial Variability of Methane Emissions in a Northern Valley Fen Ecosystem." *Biogeosciences* 17 (23): 6247–6270. doi:10.5194/bg-17-6247-2020.

Zimmermann, B., and A. Kohler. 2013. "Optimizing Savitzky–Golay Parameters for Improving Spectral Resolution and Quantification in Infrared Spectroscopy." *Applied Spectroscopy* 67 (8): 892–902. 10.1366/12-06723. doi:10.1366/12-06723.